



## Determination of unstable tectonic zones in C–North deposit, Sangan, NE Iran using GPR method: importance of structural geology

A. Rezaei<sup>1</sup>, H. Hassani<sup>1\*</sup>, P. Moarefvand<sup>1</sup> and A. Golmohammadi<sup>2</sup>

1. Department of Mining and Metallurgy Engineering, Amirkabir University of Technology (Tehran Polytechnic), Tehran, Iran  
2. Geological Survey and Mineral Exploration of Iran, Tehran, Iran

Received 19 August 2018; received in revised form 22 December 2018; accepted 14 January 2019

### Keywords

*Geological Structures*

*Ground Penetrating Radar*

*Resistivity*

*Modeling*

*C-North Deposit*

*Sangan*

*Iran*

### Abstract

Ground Penetrating Radar (GPR) is an effective and practical geophysical imaging tool with a wide set of applications in the geological mapping of sub-surface information. This research work aims at the determination of the geophysical parameter differences in the sub-surface geological structures and construction of a 3D fracture model. The GPR and resistivity methods are applied to detect the unstable tectonic zones in the C-North deposit. The structural geology investigations are first surveyed to detect the faults and fractures in the studied area. Based on the structural features, the survey is conducted over an area of 1 km<sup>2</sup> with a total of 30 profiles for detection of low-resistivity zones in the C-North deposit, which is of great help in reducing their impacts in slope stability studies. The GPR sections are then obtained from low- and high-frequency antennas (10 and 50 MHz) to detect the fractures and water content zones. The results obtained demonstrate that the major structural trends in the studied area are W–E, NE–SW, and NW–SE, while the fault zones can create pathways for groundwater inflow into the deposit in the future. The information obtained from the geological and GPR studies are also integrated with the drill hole data. The geological information from the structures are in good agreement with the actual geological situation. The method and results of this work could be useful in solving the problems related to the sub-surface structures in mining engineering.

### 1. Introduction

The structural features such as faults and fractures have a significant role in the transportation of hydrothermal fluids during the mineralization processes. The faults and fractures offer pathways of least resistance for magma to ascend and erupt [1]. These discontinuities are the critical factors that determine the quality of rock masses such as the strength of rock structures or the flow characteristics of rock masses [2-4]. Rock mass is typically characterized by inherent fractures that cause natural blocks of rocks, and rock mass fractures control the feasible exploitation and stability of benches [5]. Thus an accurate sub-surface detection and modeling of fractures is required for the pre-exploitation evaluation and planning. The recent remote fracture detection

methods could solve the accessibility problem, which is significant for application of fracture detection to the landslides and rock slope stability analysis [5]. The complexity of the intersections of structural discontinuities and the mechanical properties of rocks contributes to the formation of sliding surfaces in the mining regions. In the slope stability evaluation, the development of a complete geotechnical model that consists of four interlinked components (geology and structure of the ore body, and open-pit rock mass characteristics and hydrogeology) can prevent such hazardous incidents from happening. According to the deformation mechanism of rock slope and engineering geological and hydrogeology conditions, the important factors

✉ Corresponding author: [hhassani@aut.ac.ir](mailto:hhassani@aut.ac.ir) (H. Hassani).

influencing the stability of rock slope are summarized as the quality of rock mass, rock mechanical properties, rock mass structure of the slope, groundwater conditions, slope angle, failure mode, dip of slip plane, sliding plane types, landslide inducing factors (rainfall and groundwater), etc. The characteristics of the rock mass are not only influenced by rock mechanical properties but also are constrained by the geometric distribution of the fracture planes [6, 7]. Due to the optimization in cost and time, the application of geophysical methods has recently been increasing in the mining activities. The geophysical techniques can give a realistic 3D image of fracture spatial orientation by applying a 3D in-situ cheap data acquisition. The Ground Penetrating Radar (GPR) technique has applications in fracture detection within resistive rock masses and discontinuities and other defects such as voids and clay intrusions [8]. As a quick, non-destructive and cost-effective tool, GPR has been used in the mining industry for various purposes [9]. In particular, GPR is a useful tool for estimating the physical characteristics of a medium in several geoscience and engineering applications and also for investigating the subsurface anomalies when the tool is applied in an appropriate environment [10]. GPR can enhance fractured rock description by providing spatially continuous sub-surface information. Application of the GPR technique in mining is broad due to the complexity of geological environments required to interpret often subtle textural variations in radar data to relegate the application to experienced users [11]. GPR currently operates on mining sites as a tool to deliver comprehensive analysis resulting in detailed verification, structure mapping, and mine planning. For all of these GPR applications, estimating the velocity of propagation of electromagnetic waves in a medium or the dielectric constant of a medium is an important parameter for two main purposes: i) to detect sub-surface anomalies in a true sub-surface depth and migrate diffractions to be focused in their correct geometric shapes [12]; ii) to estimate hydrogeological parameters of soil or rock medium such as water content and porosity [13]. In such a context, the GPR method has been proven to give accurate results to characterize faults by identifying offsets of radar reflections and deformation along the strike of the fault [14-17]. Recently, custom-designed GPR instruments have been trialed on iron ore resource definition projects with results ranging from no

penetration to excellent resolution to over 100 m, depending on the ore and setting type [18]. GPR investigations serve as the basic information for the mine designers who need to understand the distribution of discontinuity systems, location of sub-surface fractures, and groundwater conditions in the mining region to select the best exploitation method. It can also reduce drilling costs of providing high-resolution continuous delineation of geologic structures.

In this research work, we used the GPR method, given that it is a fast and non-invasive method to detect subsurface unstable tectonic zones. The objective of this study was to determine the sub-surface geologic structures and the characteristics of the water content based on the GPR and resistivity surveys and the available structural data. Another aim of this research work was a 3D deterministic unstable zone modeling approach using GPR as a data acquisition tool in the C-North deposit of Sangan.

## 2. Methods

A structural study typically pertains to the observation, description, and interpretation of the structures that can be mapped in the field. A geostructural survey devoted to a systematic and quantitative description of rock discontinuities is a fundamental part of the study of the stability conditions of a rock mass [19]. In the mining works, a better knowledge of the detailed structural work is required. A method for rock discontinuity mapping that relies on accurate high-resolution survey technologies was developed in this work.

The GPR measurements are based on transmitting electromagnetic waves into the rock media. The propagation of these waves is mainly controlled by the dielectric properties of the media. The electrical boundaries are created at the interfaces of the geological materials with different dielectrical properties [20, 21]. Estimating the velocity of propagation of the electromagnetic waves in a medium (or the dielectric constant of a medium) is a significant parameter used to convert the measured traveling time of the reflections into the true sub-surface depth [22]. Estimation of the representative dielectric constant of the rock medium was carried out using the “depth of known reflector” technique [23, 24]. According to Daniels (2004), the velocity of propagation of electromagnetic waves in the rock depends on the relative permittivity, which is correlated to the porosity and water content [25].

The attenuation of the GPR pulse is also affected by the conductivity and dielectric effects, and is correlated to the frequency of the waves [26]. The resolution, depth penetration, and detection properties of GPR depend on the antenna frequency used. The frequency selection of the antenna depends on the surveying objective. Low-frequency antennas provide a large penetration depth but in a less detail, whilst high-frequency antennas provides a more detailed sub-surface image but a lower penetration depth [25, 27]. There are other factors such as the water content and homogeneity of the medium that control the signal penetration depth. It reveals the physical discontinuities, like faults and fractures, of the rock mass, where the dielectric properties change enough to give a reflection of the radar wave transmitted by the GPR antenna. Such surveys are ideally suited to low-frequency flexible towed in-line antenna systems [10].

The GPR measurements can be interpreted as single profiles but can also be used for a 3D modeling. Since GPR detects physical discontinuities, a good geological knowledge of the site and data from other investigation methods such as diamond drill cores is required for interpreting the features of the GPR data. The advantage of the method is its acceptable vertical and lateral resolution in high resistivity environments. Most mining applications require antenna center frequencies in the range of 10-50 MHz [5]. Measurements with a low-frequency antenna can be done since they are less affected by the surface materials. The electrical conductivity value is vital in understanding the sub-surface condition as each type of soil or rock has specific electrical properties. The electrical conductivity value is measured using the geophysical methods like GPR and 2-D resistivity imaging.

To get the most reliable results, we used only the probe locations, where a GPR trace was available. We extracted the one-way travel time from the raw GPR data for the traces, where we made probe measurements based on the recorded 'GPR time' that allowed us to look at the exact trace of interest. The use of a new equipment that collects data rapidly was found to be especially useful for creating the 3D models of the data. A 3D structural modeling of the sub-surface is a major instrument in geosciences that helps visualizing, understanding, and quantifying the geophysical processes.

The data used for the GPR survey and its interpretations consists of the geologic map scale

of 1:2000, topographic map data, structural survey, and drill hole log information. In this research work, the integration between the GPR results, field observation, electrical resistivity values, and drill hole log produced more reliable information about the studied area.

### 3. Studied area

The Sangan iron skarn complex is one of the most important deposits associated with the Tertiary volcanic-plutonic magmatism in NE Iran. The studied area is located in SE of the Khorasan-e-Razavi Province, approximately 280 km from the City of Mashhad, and in the end part of the Khaf-Kashmar-Bardskan Tertiary magmatic belt of Central Iran blocks along the regional E-W trending and the eastern segment of large scale old Doruneh fault passing near the area that lies between the longitudes 60° 10' 00" to 60° 50' 00" E and the latitudes 34° 20' 00" to 34° 40' 00" N (Figure 1a). The Sangan Magmatic Complex (SMC) at the NE edge of the Lut block includes a thick pile of volcanic rocks intruded by younger granitoid stocks [28]. SMC includes several ore bodies in the east-west direction. Based on the characteristics of the ore deposits, this mining region is divided into western (sub-divided into the A, A', B, CS (C-South), CN (C-North)), central (sub-divided into Baghak (BA), and Dardvey (D)) anomalies (Figure 1a), and the eastern anomaly (sub-divided Senjedak 1, 2, 3; Madanjoo, Som-Ahanai, and Ferezhneh). The Sangan iron skarn deposits are distributed along the contact zone between the Jurassic clastic rocks or Cretaceous carbonates and the Eocene igneous rocks (Figure 1b) [29].

### 4. Geology of studied area

SM, is located in the eastern part of the Sabzevar Doruneh Magmatic Belt (SDMB) consisting of intermediate to felsic intrusive and extrusive (volcanic and pyroclastic) rocks, and at the eastern edge of the Khaf-Kashmar-Bardskan Volcano-Plutonic and Tertiary Metallogenic Belt (KKB-VPMB) in NE Iran [30]. The oldest geologic units in the Sangan region include Precambrian schist and Paleozoic metamorphic rocks, which are overlain by a complex assemblage of Eocene volcanics, Oligo-Miocene sedimentary deposits, and Jurassic and Cretaceous formations (Figure 1a). The metasedimentary rocks represent the oldest rock units. The oldest unit is a thick pile (1500 m) of sedimentary rocks that consists of lower Jurassic shales and siltstones, which are overlain by Upper Jurassic to

Cretaceous limestone, dolomite, and rare gypsum [31]. The whole rock sequence up to the upper Eocene is intruded by the Late Eocene granitoids [29]. The carbonate rocks of Jurassic consist of crystalline and less dark dolomite limestone that spread all over the area [32]. This sedimentary sequence is either intruded by granitoids or is unconformably covered by volcanic rocks. The depressions between the ranges are filled by thick Neogene sediments. Granitoid rock intruded older rocks such as crystalline limestone and dolomite and volcano-sedimentary rocks in the pre-carbonifer age, and quartzite, slate, and

conglomerate in the carbonifer age. Granites and syenogranites are two main intrusive rocks exposed in the studied area [30]. Syenogranites are widespread in the north of SMC and exhibit porphyritic textures with a weak alteration consisting of sericite and chlorite [28]. The structural features of the region such as faults and foldings, as well as the strike of the formations follow the E-W to NW-SE direction of the major Doruneh fault [30]. As stated earlier, occurrences of iron are present in several places in the studied area including small and large bodies of magnetite in relationship with skarn-type rocks.

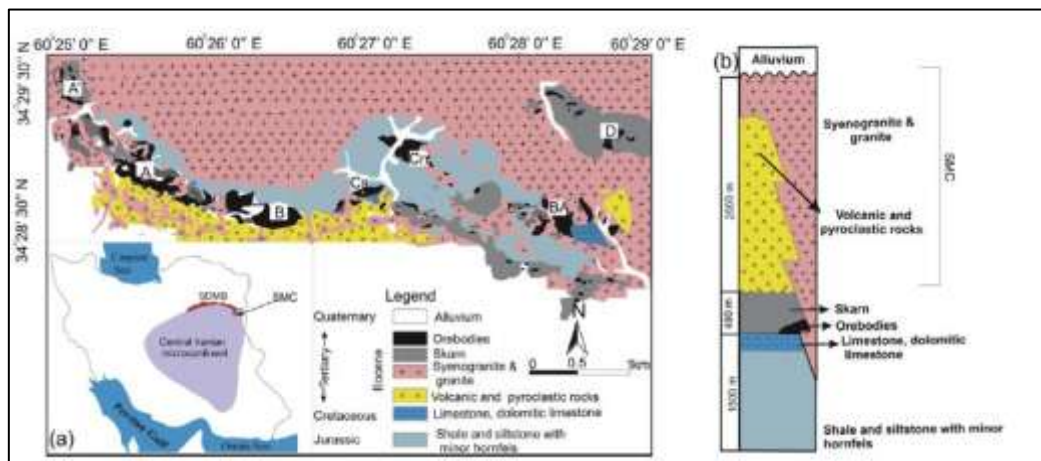


**Figure 1. (a) Map of Iran and geological map of the Sangan region including location of the Sangan deposit and the Eocene plutonic and volcanic rocks based on 1:250,000 geological maps of Taybad [33]. Simplified geologic map of the western (A', A, B, C-South (Cs), and C-North (Cn)), and central (BA, and D) anomalies are shown; (b) Stratigraphic columnar section of the Sangan area [34].**

## 5. Discussion

### 5.1. Structural analysis

The C-North deposit is one of the most important western deposits in the Sangan mining region. The slope stability in open-pit mines is controlled by the persistence and characteristics of discontinuities such as beddings, faults, and major joints. The spatial distribution of collapse in open-pit mines positively correlates with the distribution of discontinuities, and hence, the structural instability is significantly influenced by discontinuities [35]. In this section, we focused on the structural and geological properties of the C-North deposit in order to explore the possibility of slope failure during mining operations with the goal of investigating and characterizing the geological structures in the area. In order to reach this goal, the dip direction, dip, and location of each fault were obtained. Many faults were identified in different rock outcrops based on field observations. The data used for this research work was field data including the dip direction/dip of faults in the C-North ore deposit. Based on the

field data, a total of 16 major faults (often normal) were measured throughout the studied area in order to perform a detailed structural analysis (Table 1). This data was analyzed using the stereonet for classification of faults and their evolution. Dip direction showed more variations. In the studied area, there were a variety of discontinuities such as strike-slip and normal faults, and tensile major joints with a considerable aperture. Figure 2 presents the stereography of faults including pole plot and rose diagram in the C-North deposit. The resulting rose diagram showed the dip direction frequency of the faults. According to the rose diagram (Figure 2a), the dominant structural trends were W-E, NE-SW, and NW-SE, and the result of local stress redistribution caused by the NW-SE fault structure (Dardvey fault). The two groups of faults of different ages that constitute the fracture system of the region contrast sharply in general character, and continuity and apparently formed from different stress patterns. The older fault sets are persistent widely-spaced fractures or zones of

fractures; several W-E trending faults can be traced for several kilometers outside the mineral belt. The fracture distribution within the ore deposit is in relation to the dominant compressional and tensional stresses in the studied area. These fractures must have developed from regional stresses that affected most or all of the reserve of Sangan. The younger faults, on the other hand, are relatively discontinuous, closely spaced, intersecting fractures that seem to be nearly restricted to the mineral belt. These faults were probably formed from regional compressive forces. This geological structural information helps us to select target areas to conduct the GPR survey.

Also major structural features were interpreted from the field observations of the area and their special relationship with the mineral deposits. The faults were used to prepare the fault map using the fault density (FD) equation [36]:

$$FD = (a / A) + (b / B) + (c / C) \quad (1)$$

where

a: is the number of the linear structures in the selected cell size; A equals the average number of all lineaments in the entire map; b is the length of the linear structures in the selected cell size; B is the average length of all the faults in the entire map; c is equal to the number of the intersections of the faults in the selected cell size; and C is the average number of total intersections in the entire map. To build this map, the region was derived into separate cells with appropriate dimensions (50 m in this work). After computation of the numerical amounts of the proposed cells, the final FD map of the area was prepared (Figure 3). The inferred relative age of the different fault sets is as follows: the E-W fault set is the oldest in the area, followed by the NE-SW fault set, then N-S set, and finally, the NW-SE set. The criteria used for the definition of the relative age is direct observation of cross-cutting relationships between faults of different sets.

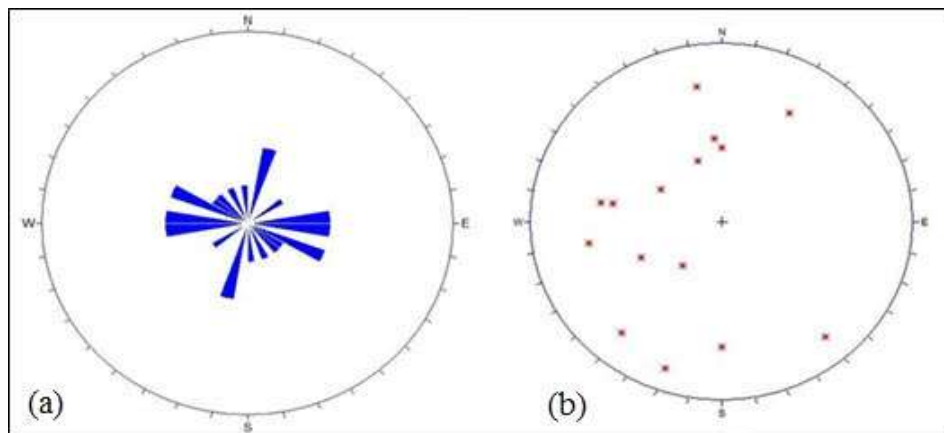


Figure 2. Statistical analysis of fault data in the C-North ore deposit; a) rose diagram, and b) pole plot.

Table 1. Specification of faults in the C-North deposit.

Fault No.	Fault dip direction	Fault dip
F1	N120°	40°
F2	N65°	50°
F3	N40°	35°
F4	N20°	82°
F5	N20°	82°
F6	N40°	78°
F7	N100°	65°
F8	N180°	45°
F9	N360°	70°
F10	N100°	60°
F11	N320°	80°
F12	N80°	70°
F13	N210°	70°
F14	N170°	75°
F15	N175°	50°
F16	N160°	40°

### 5.2. GPR survey and data processing

The GPR survey was conducted during February and March 2017 over an area of 1 km<sup>2</sup> with LOZA-V antennas. Low-frequency GPR antenna (10 and 50 MHz) was used to obtain a deep image of the sub-surface. The objective of using a low-frequency antenna is to obtain as deep a sub-surface image as possible since the penetration depth is inversely proportional to the wave frequency. The 10 MHz antenna was used to map the deepest discontinuities, while 50 MHz was used for higher resolution studies of the shallower parts. The zones of the potential existence of geological features were designated for the GPR survey. GPR profiles were designed for the occurrence of lineaments such as different types of faults and fractures. We tested the ability and quality of low-frequency GPR antenna to image fracture as a greater depth in a case study. Using the GPR method, we aimed at determining

the presence of subsurface structures and the discontinuities along which they could develop.

A total of 7 km long from 30 GPR profiles present within different horizons was measured in the C-North ore deposit. The GPR data from the C-North ore deposit was collected from several localities. The studied area was divided into 30 profiles with variable lengths, while the localities were selected based on the structural analysis results. Figure 4 displays the location of the GPR profiles in the studied area. Specification of the GPR survey profiles in the C-North ore deposit is presented in Table 2.

We carried out the GPR survey and the interpretation of GPR profiles, and correlated them with the results of the detailed structural mapping of the studied area. However, their correlation with geological and structural data gave a more precise insight into the structural setting of the studied area.

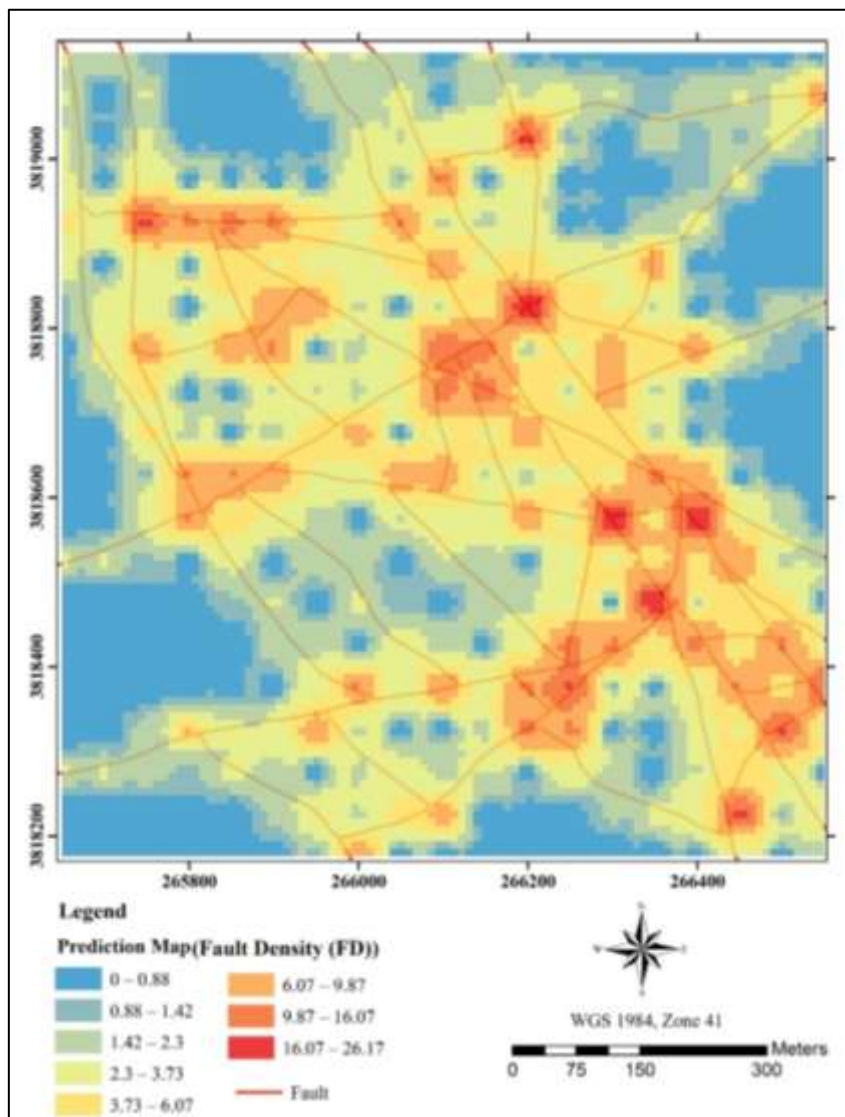


Figure 3. Map of fault density (FD) by the Inverse Distance Weight (IDW) method for the studied area.

The GPR data is usually processed at the time of measurement to provide the possibility of evaluating the results on the field. Due to the large volume of data acquired from the field, an effective maintenance of the data was required to ensure good data quality, and interpretation was maintained [37]. The data processing consisted of filtering to reduce noise (including high pass, low pass, and spatial filters for clarifying the picture to enable a better detection of the reflections); topographic correction to compensate for changes in surface elevation; and depth conversion [38]. The processing methods were applied to the data with caution so as not to remove the essential characteristics of the rock. The RadExplorer 1.4 software from DECO Geophysical was applied for the GPR data processing [39]. We defined the geometry of profiles by entering the coordinates of the start and end points of profile lines. Since the data was acquired with the time trigger and since maintaining a steady pace while measuring is not always possible, spatial interpolation was applied first. This process recalculates the data with the interpolation of traces in the horizontal direction [39]. This enabled the program to calculate the distances between the traces that was necessary for a proper functioning of some processing routines used later in the process [39]. During the GPR survey, the 30 profiles of the C-North deposit was considered, and the data of GPR cross-sections along these survey lines was recorded. In the profiles, the vertical or sub-vertical fracturing can also be linked to the GPR measurement data, helping the interpretation of the results.

Integration of the GPR method and geological survey results led to the determination of mining parameters important in the slope stability analysis. The data gathered through geological surveys was used for interpretation of the GPR data. The results of data processing and the geological interpretation models for each profile were separately described. The positions of the geological features derived from geophysical surveys were compared with the geological maps and drill hole log of the studied area. The results obtained allowed to verify the location of the mentioned structures imposed on geological maps, and to conclude on positions of selected lineaments in areas of where the data was not available yet. In the following section, the GPR and geological interpretation results are presented for the most significant profiles in the C-North deposit. GPR is also useful in interpreting whether fractures are continuous or if the fractures, e.g. in

adjacent drill holes represent different fracture planes. The characteristics of the fractures such as openness can be observed from vertical rock faces or surface mapping information and then used in the interpretation of the GPR profiles. In this research work, we also calculated water content for all the high-density probe measurements. The electrical conductivity value is obtained using the GPR and 2-D resistivity methods.

30 radargrams were carefully investigated in order to determine the required signal processing functions. Using the RadExplorer 1.4 software, the reflected data was processed, leading to enhancing the signal and clarifying the reflections in the cross-sectional radargrams. Also resistivity surveys were carried out along the GPR survey lines. In this work, only the 50 MHz radargrams were considered since this frequency provided enough penetration depth with a higher resolution compared to the 10 MHz radargrams.

In this work, the sub-surface tectonic evolution of the C-North deposit was studied using GPR profiles-five of these (S12, S24, S25, S26, and S27) were selected for illustration-supported by the drill hole log in the studied area. We correlated the GPR results with the results of structural and drill hole log by constructing five GPR cross-sections.

**Table 2. Specification of GPR survey profiles in the C-North deposit.**

Profile number	Length (m)	Strike
S01	100	W-E
S02	250	NW-SE
S03	250	NW-SE
S04	150	NW-SE
S05	100	NW-SE
S06	270	NW-SE
S07	270	NE-SW
S08	125	N-S
S09	115	NE-SW
S10	150	NW-SE
S11	150	NE-SW
S12	600	N-S
S13	200	W-E
S14	130	N-S
S15	140	W-E
S16	150	W-E
S17	250	N-S
S18	240	NE-SW
S19	350	NE-SW
S20	310	W-E
S21	265	W-E
S22	190	NE-SW
S23	350	N-S
S24	550	NE-SW
S25	550	NE-SW
S26	143	NE-SW
S27	125	NE-SW
S28	300	NE-SW
S29	175	NE-SW
S30	250	NW-SE

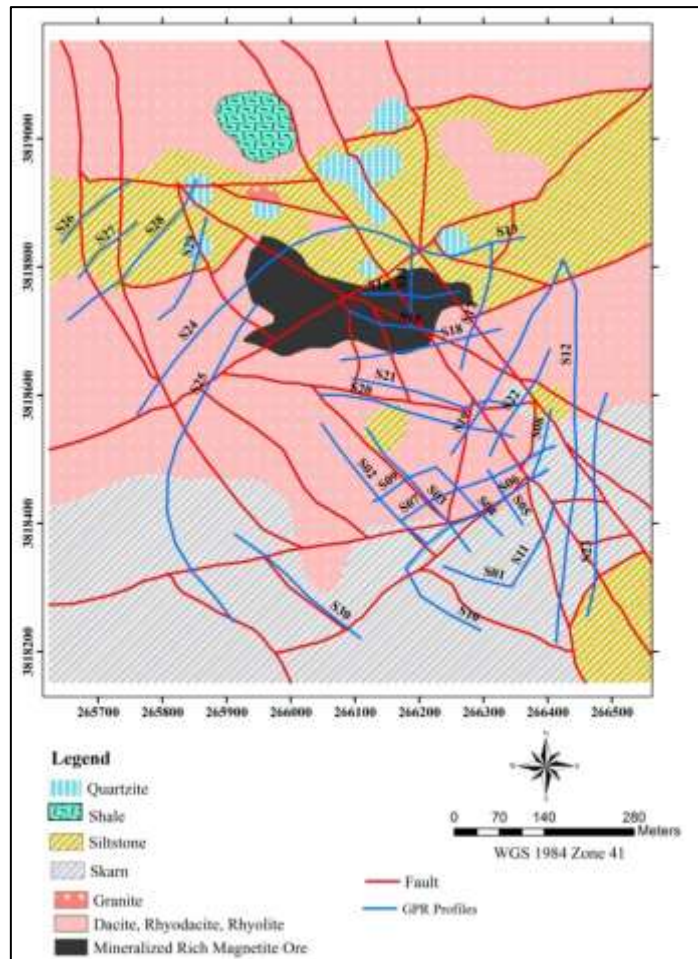


Figure 4. Map presenting the GPR survey lines in the C-North deposit.

### 5.2.1. Profile S12

The 2-D-interpreted GPR and resistivity sections passing through near the eastern part of the studied area in a N-S direction is shown in Figure 5. This profile is approximately 600.0 m long, and displays the sandstone and rhyodacitic geological units in the studied area. Several fractures were distinguished by the interpretation of this cross-section (red dashed line) (Figure 5a). The detection of vertical fractures by GPR is emphasized in the results of the combined GPR profiles and the observations of the fractures. Low-resistivity zones have been developed along some of these fractures (white halos) (Figure 5b). The main reasons for the resistivity reduction in these zones include the penetration of rhyodacitic masses and alteration of the host rock. Water content variations indicate that the saturation zone develops from a depth of 45 m along the profile (Figure 5c).

### 5.2.2. Profile S24

This profile was surveyed in the northern-western part of the studied area in a NE-SW direction. The profile length was 550 m. In this section, the

lithological units consist of sandstone and shale. The results of the GPR and resistivity surveys are shown in Figure 6. The most important structural feature in this profile is the intersected fractures (red dashed line). Beside these fractures, a large number of separate minor fractures distributed along the GPR section are clearly seen in this profile. The resistivity result delineated an alteration zone with a low-resistivity of 300 to 360 m of the profile that could create pathways for groundwater drainage into the mine pit. Furthermore, another zone is separated from 450 to 500 m, which is associated with reduction in the resistivity and a relative increase in the water content (Figures 6b, c).

### 5.2.3. Profile S25

The 2-D-interpreted GPR and resistivity surveys in profile S25 passes through near the western part of the studied area in an NE-SW direction, while the lithological units are sandstone and dacitic mass (Figure 7). In this GPR profile, we were able to determine the discontinuity along which it developed (Figure 7a). We can observe the low-resistivity zones along the profile (Figure 7b).

**5.2.4. Profile S26**

This profile is located in the western part of the studied area in an NE-SW direction. It is about 150.0 m long, and the geological units are shale, sandstone, and rhyodacitic masses. The most remarkable feature in this profile is the intersected fractures (Figure 8a). One of the reasons for decreasing resistivity is alteration of the host rock in profile S26 that is eventually introduced as unstable and tectonized regions (Figure 8b).

This profile is located in the western part of the studied area, and it is parallel to S26. The length of S27 is about 140 m. The main lithological units are sandstone and rhyodacitic masses. Several fractures were determined by interpretation of this cross-section (Figure 9a). Two alteration (low-resistivity) zones are observed in the initial and the end sections of the profile (Figure 9b). The two main reasons for the wall instability in the western part of the ore deposit include the alteration zones and the increasing value of water content (Figure 9c).

**5.2.5. Profile S27**

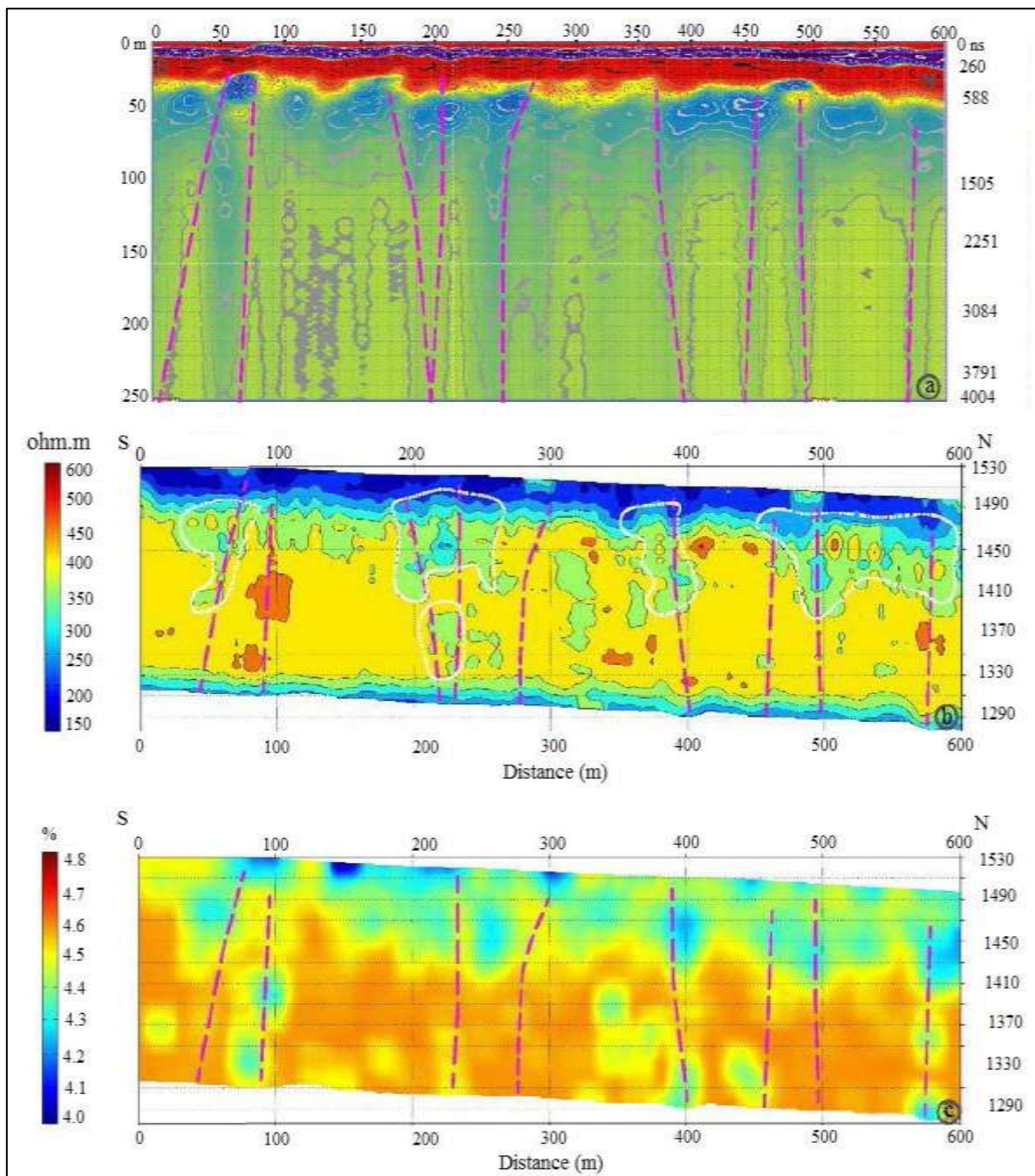


Figure 5. GPR reflection section and the interpretation model from profile S12 in the C-North deposit (5a: radargram, 5b: electrical resistivity, and 5c: water content).

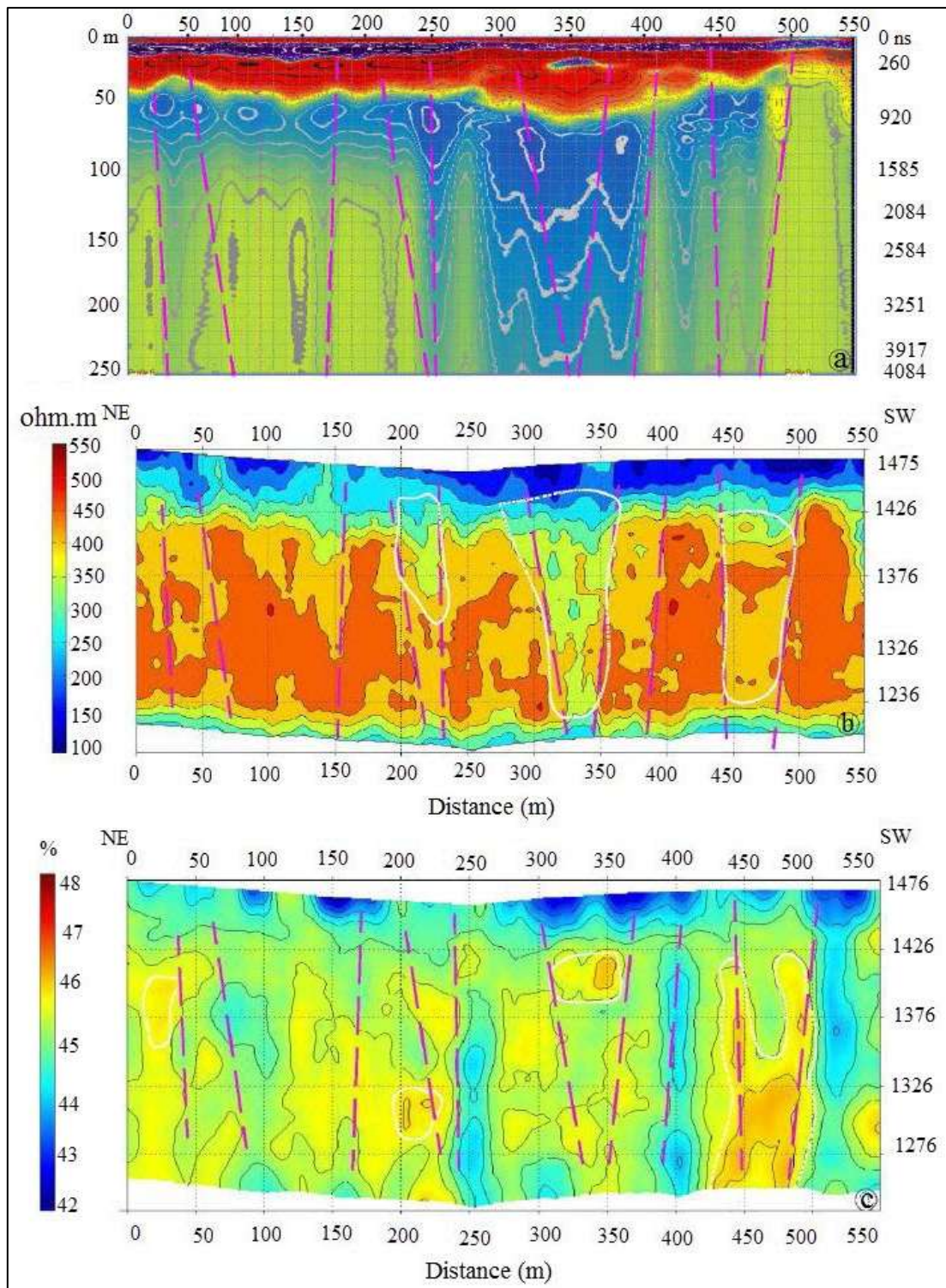


Figure 6. GPR profile from survey profile S24 along the northern boundary in the C-North deposit (6a: radargram, 6b: electrical resistivity, and 6c: water content).

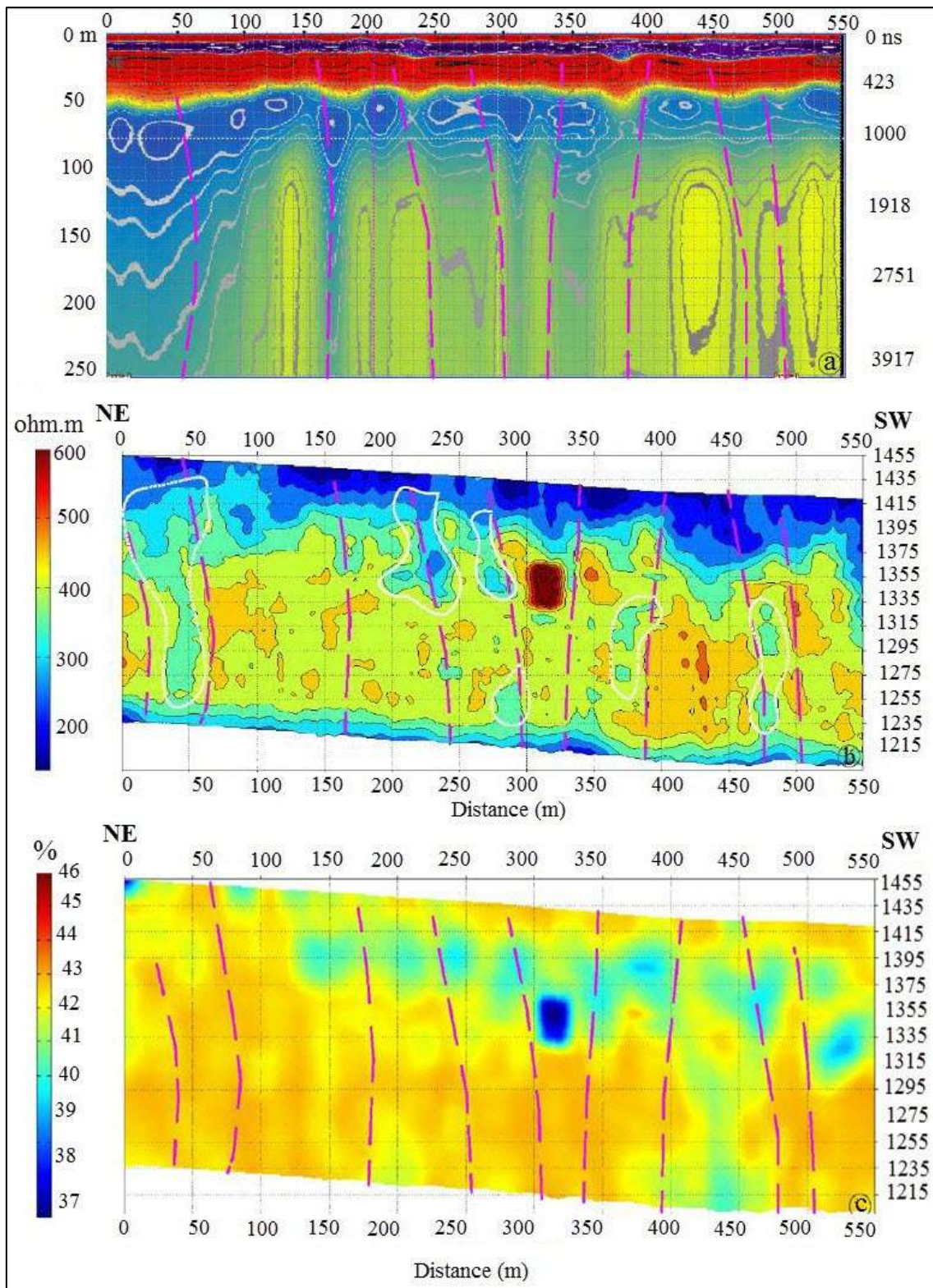


Figure 7. GPR reflection section and the interpretation model from profile S25 in the C-North deposit (7a: radargram, 7b: electrical resistivity, and 7c: water content).

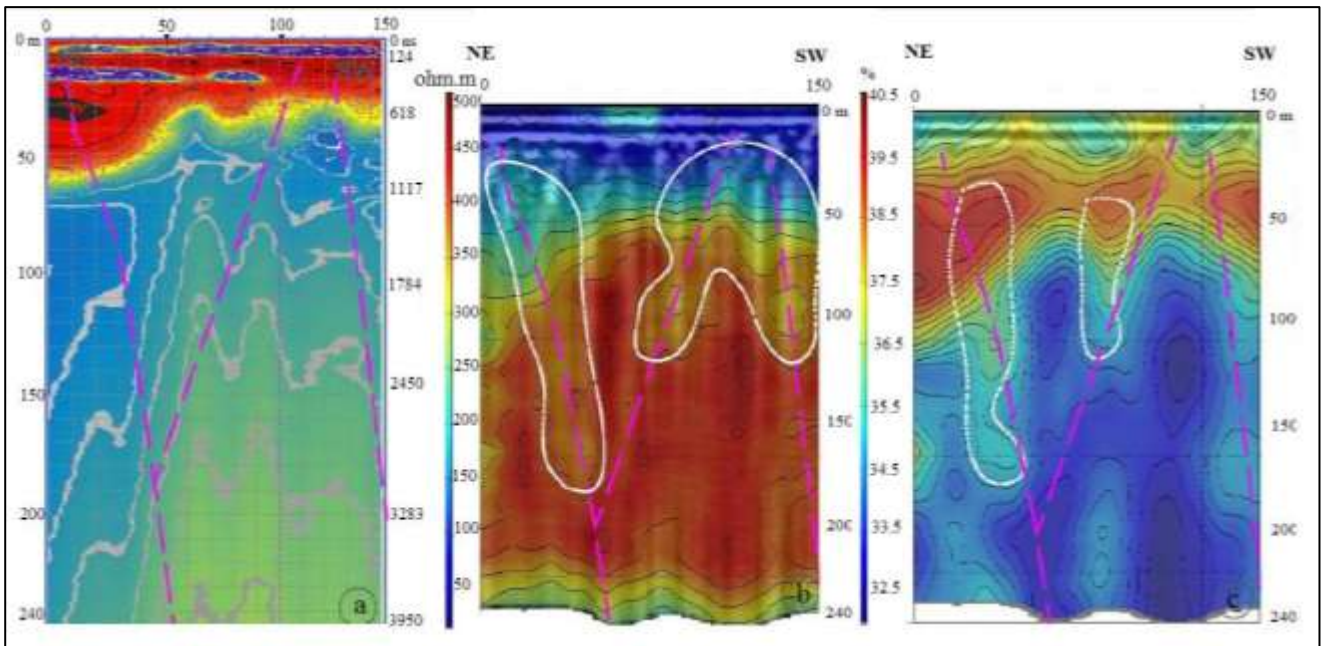


Figure 8. GPR reflection section and interpretation model from profile S26 in the C-North deposit (8a: radargram, 8b: electrical resistivity, and 8c: water content).

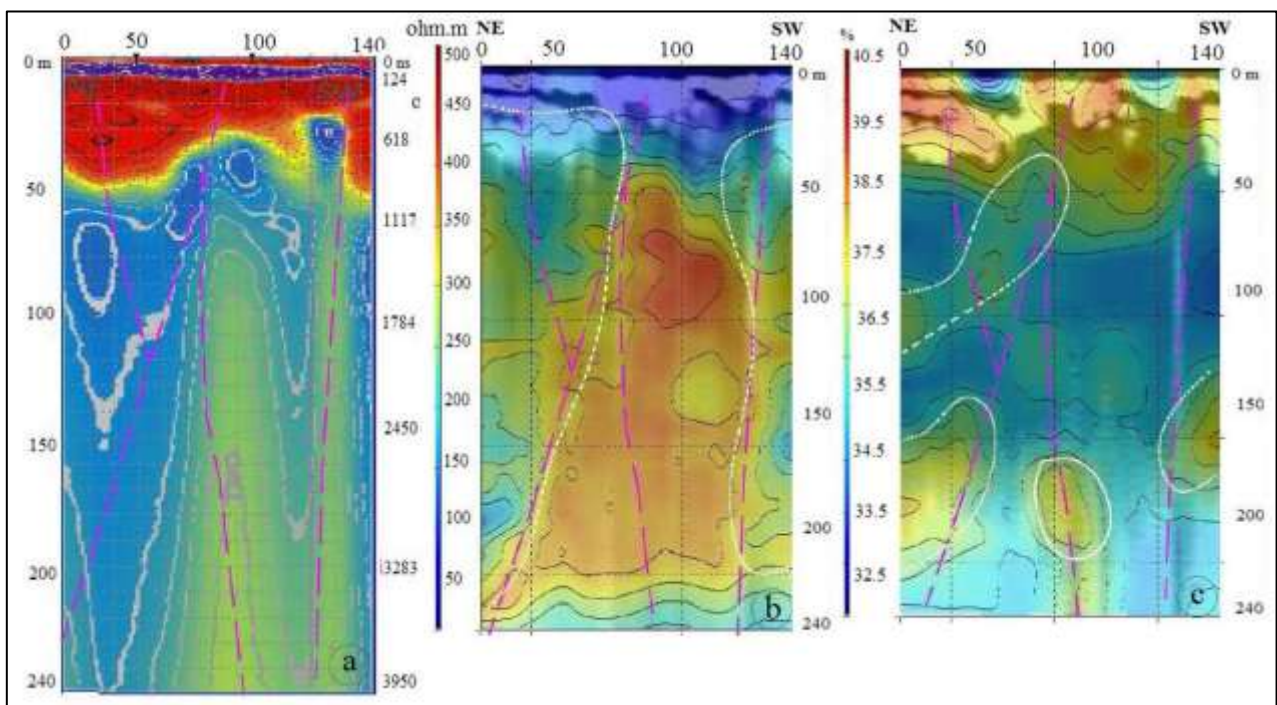


Figure 9. GPR reflection section and interpretation model from profile S27 in the C-North deposit (9a: radargram, 9b: electrical resistivity, and 9c: water content).

In this section, we should confirm the presence of discontinuities with the interpretation of GPR profiles and correlate them with the results of detailed structural mapping (sub-surface) in the studied area.

A comparison between the orientations of the fractures measured through the traditional manual survey and the orientations of the modeled fractures is presented as a possible geologic

validation for the detection and interpretation of fractures. For the objective of pre-exploitation evaluation, a distribution analysis study of fractures allowed to obtain an evaluation-based fracture index for the bench of the case study. To validate the geophysical results, the sub-surface data (drill hole log) and field observations were used.

The results of the core drilling can be used in the interpretation of the GPR measurements, especially in the detection of fractures of different magnitudes. In other words, GPR can be used as a method whereby observations of fracturing and general soundness from mapping and core drilling can be extended into larger rock volumes. We studied the sub-surface structural features based on the drill hole log information since we could compare them with the results of the GPR interpretation. In order to observe the spatial distribution modeling in two dimensions in the studied area, one geological cross-section in the

N-S direction on the basis of sub-surface data was drawn containing the drill holes that take place in the ore zone areas (Figure 10). The open fractures intersecting in the drill cores were in the GPR data. The combination of geological results, GPR interpretation and drill hole log shows that there are many unstable zones in the studied area. Such discontinuities were detected in most of the studied profiles. The results of this research work showed that the fracture zones in the ore deposit developed quickly as a result of changes in the initial stress-strain state of the rock mass.

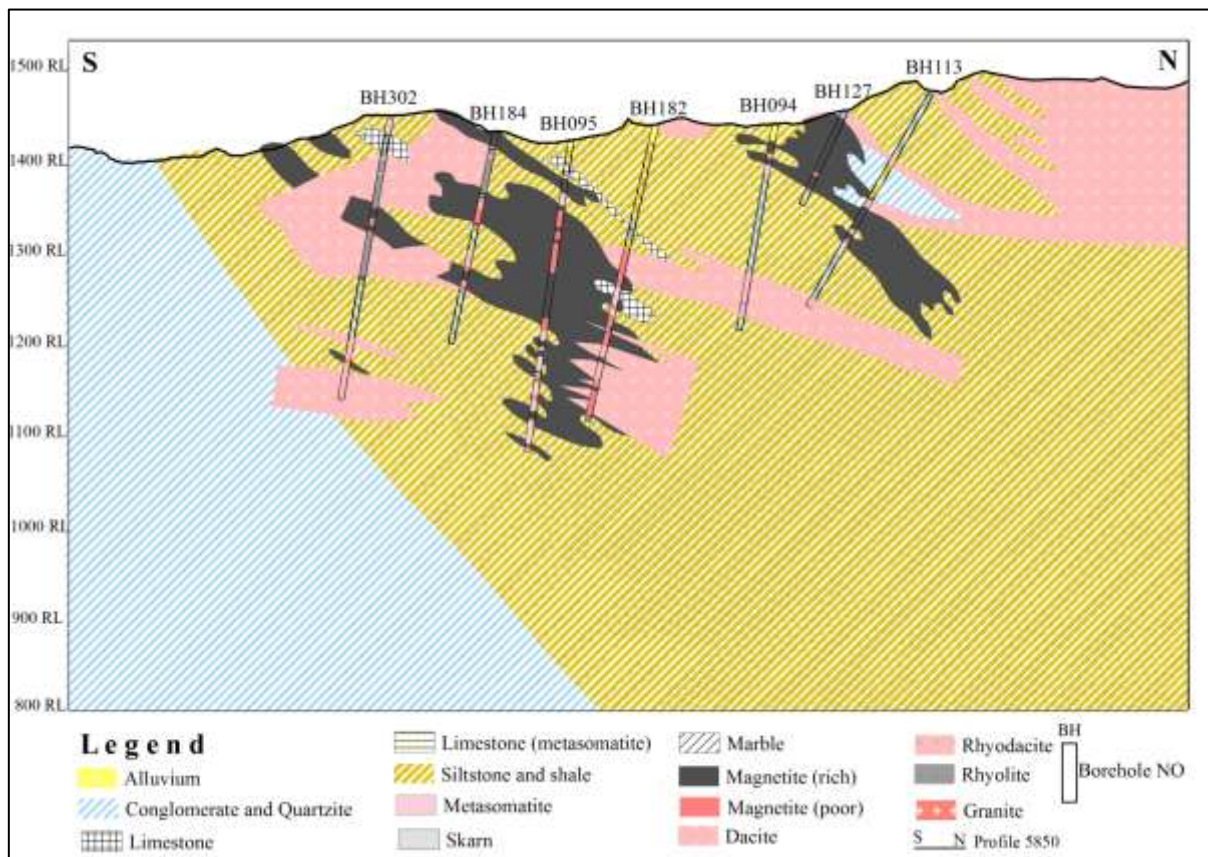


Figure 10. North-south cross-section and distribution of the drill holes in the C-North deposit.

By interpreting the GPR profiles, we not only located several fractures but also confirmed the presence of discontinuities. However, due to the limited vertical resolution of the 10 MHz frequency antenna, it was impossible to conclude whether the reflections on the recorded GPR profiles were the result of one or more parallel discontinuities. Therefore, the GPR results were correlated with the results of the structural investigations and drill hole log. In the NW part of the studied area, the surface trace of the major fault is clearly shown in the NW-SE direction (Figure 4). The data obtained from drill hole log

indicates that most of the open fractures have a similar orientation, i.e. N-NW to S-SE strike. Based on the information given and the interpreted radargrams, the degree of inclination of sub-vertical fractures is varied since some fractures are almost vertical while others are slightly inclined. As shown in the figures, the unstable zones were determined based on the GPR information and the existence of open fractures. We found that the discontinuities defined by GPR coincided with the location and dip of the mapped discontinuities, and that the observed unstable zones in the GPR profiles were located along

these discontinuities. On the basis of this work, we can conclude that the low-frequency GPR is a very efficient technique for detecting unstable zones and discontinuities. The comparison between the GPR measurements and drill hole log confirmed the effectiveness of the geophysical application to investigate the sub-surface conditions. In other words, the correlation between the discontinuity data derived from the GPR results and from the mapping of sub-surface data represents a good verification of the GPR method.

Almost all collapses of rock slopes, especially in open-pit mines are related to discontinuities such as bedding planes, faults, and major joints. These features can pose serious hazards in the mine. Since they are most dangerous when they occur at shallow depths, higher frequency antennas could

also be used to detect them and could provide an even more precise image of the subsurface. Such structures/features must be thoroughly investigated to minimize the risk of rock failure. These features can create pathways for groundwater inflow into the mine pit during mining operations. Various types of geological discontinuities are present in the C–North deposit that contribute to the fall of ground hazard; they either influence the hanging wall on their own or act in conjunction with other geological discontinuities. Figure 11 shows unstable zones in the NW part of the C–North deposit, which must be considered in slope stability studies. The red and blue dashed lines represent interpreted fractures and unstable zones along the GPR survey, respectively.

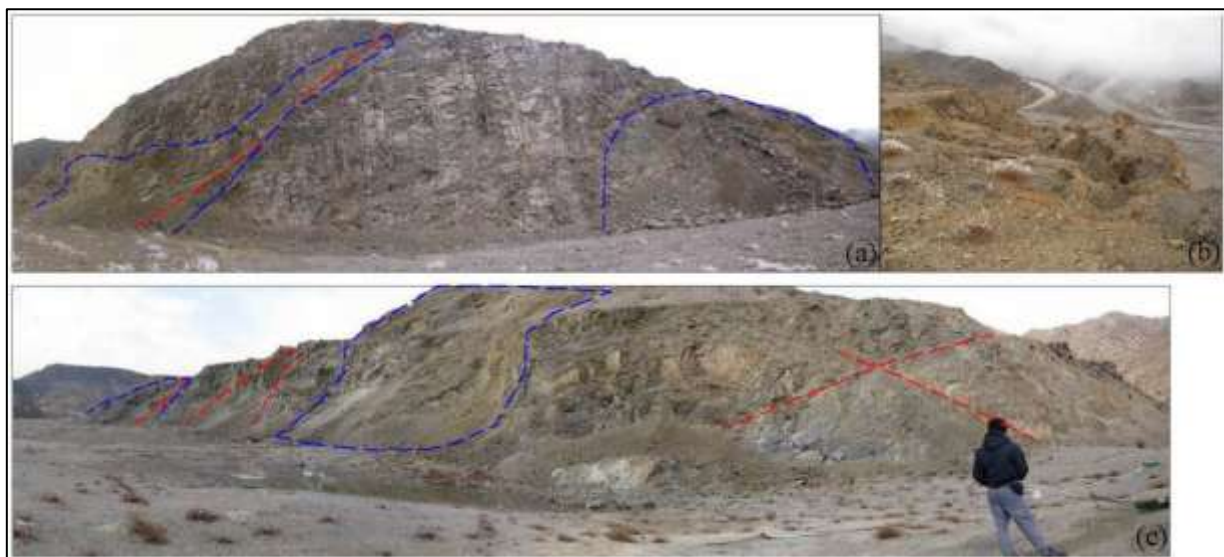


**Figure 11. View of fractures and unstable zones along profiles S26 and S27 in the C-North ore deposit (red dashed line: fractures; blue dashed line: unstable zones); a) altered and unstable zones of profile S26, b) sliding mass in downward of profile S27, c) sliding masses, altered and unstable zones of profile S27.**

The comparison of profiles at different distances from the emerging vertical structures is a good strategy to facilitate the detection of lateral reflections [40]. The results obtained from the GPR measurements were compared with surface geological and drill hole log results. The results, when viewed in their true 3D context, show the low-resistivity zones within the ore deposit, which could be due to fractures or faults and shear zones. These low-resistivity zones must be considered in slope stability studies because of having a high risk of failure. Most of the faults and fractures are steep-dipping and display vertical displacements in the C–North deposit. The application of the GPR method to determine the low-resistivity zones showed very good

results in the studied area. Figure 12 shows the position of discontinuities obtained from the GPR results which correlate well with the mapped structural discontinuities. The field observations were analyzed on the map to make an overview of the structural conditions of the deposit. Based on the rock exposed in the C-Norh deposit, interpretation of geophysical data, the relatively broad deep fracture zones are located in the NW-SE direction. The results obtained indicate that the GPR method provides a much better and more information about sub-surface than other traditional methods. Accordingly, good reflections in the GPR radargrams indicate that GPR results in this area have a high correlation with the field investigation.

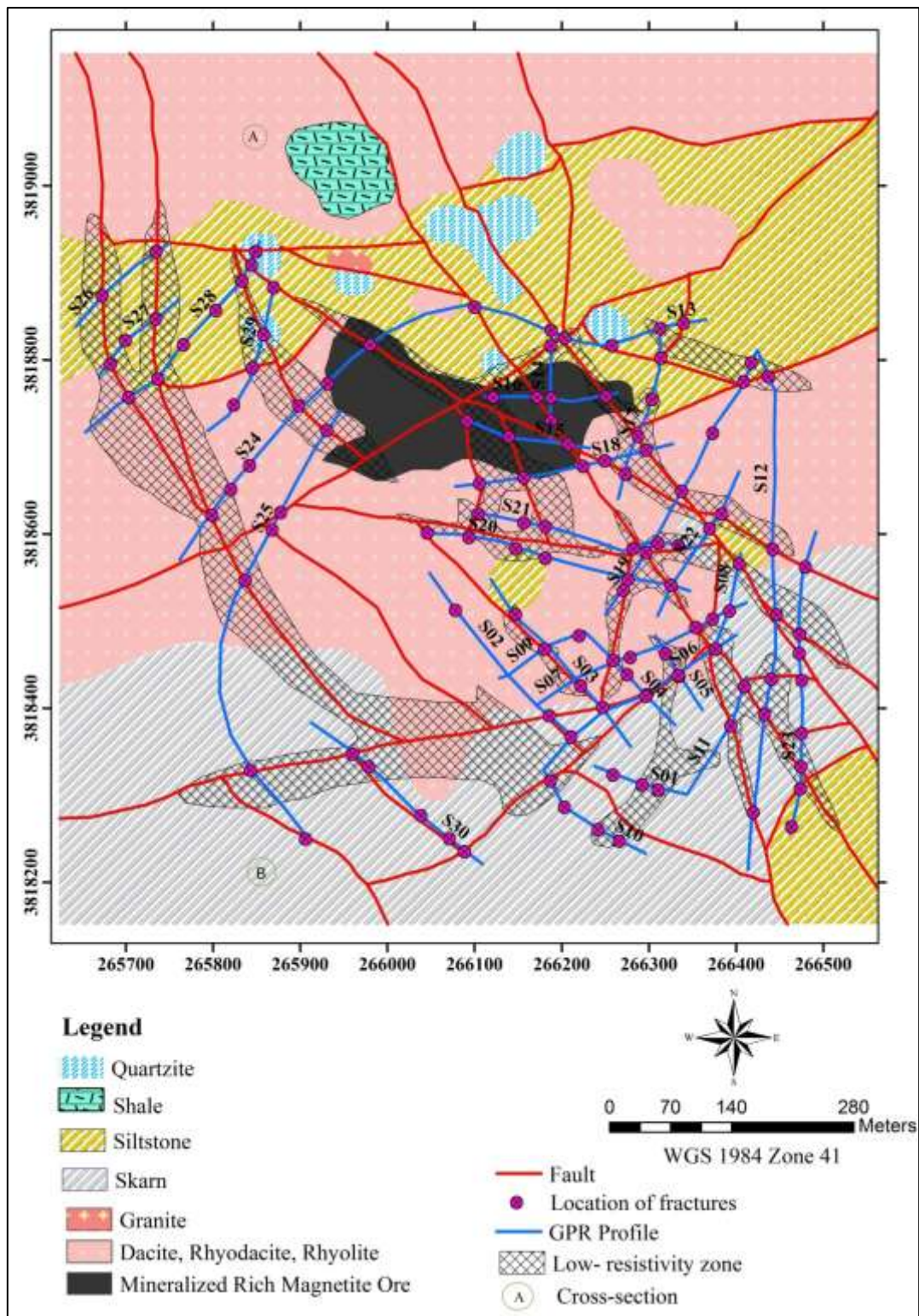


Figure 12. The primary position of low-resistivity zones and location of fractures and faults in the 2D space of the studied area.

The GPR measurements can help in correlating the fracturing observed in the drill cores over larger areas. By conducting several closely-spaced measurement profiles, the overall structure and properties of the deposit can be better understood, and for example, the fractures from adjacent

profiles can be correlated with one another. Using a measurement grid where traverses intersect each other allows the interpretation of the fracturing and its characteristics which can be visualized in a 3D visualization [41, 42]. The advantage of the 3D model is that the form and extent of the

fracture planes can be estimated and the unstable areas can clearly be seen. After standard signal processing, for the purpose of modeling the low-resistivity zones in three dimensions, the 30 2D radargrams were selected to demonstrate how unstable zones could be modeled from the GPR results in the C-North deposit (Figure 13). The 3D GPR model is based up on interpolating the data areas between the 2D radargrams in order to obtain a 3D sub-surface image for the whole body of the rock mass. This allows for a better perception of the modeled fractures in the rock mass. Visualization of unstable zone surfaces

through a graphical software can assist in exploring the spatial behavior of unstable zones in different orientations.

The fracture planes are usually curved and undulating at a scale of several tens of meters in the 3D modeling. The GPR measurements also show that the magnitude of the reflected signal from the fracture planes varies in different areas, which could be caused by the variation in the properties of the fractures or the degree of openness. The resulting 3D GPR model allows exploration of the extension, shape, and orientation of the detected fracture surfaces.

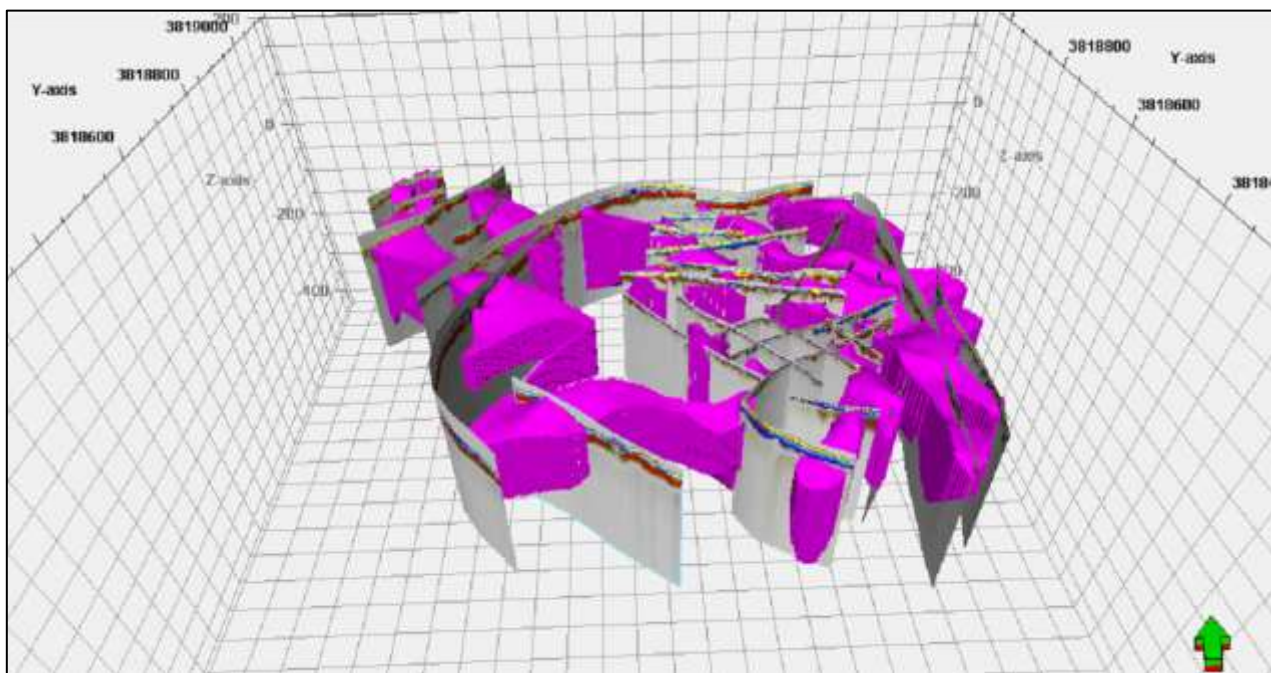


Figure 13. The 3D GPR model and distribution of unstable zones in the studied area (view of the north).

## 6. Conclusions

The structural discontinuities (fractures, joint, etc.) can not be easily and fully recognized before exploitation, and the information collected from the field is a key factor in this process. A preliminary fracture detection is a vital issue for many decisions and for design and exploitation optimization. In this work, we demonstrated how GPR could be used to delineate possible structures that host skarn mineralization in the C-North deposit of Sangam. A detailed GPR survey conducted prior to exploitation could, therefore, diminish the possibility of accidents that could happen as a result of sinking surfaces and land sliding. The aim of this work was to evaluate the suitability of the low-frequency GPR method for tracking the sub-surface structures and potential sliding surfaces or other geomechanical instabilities related to the structural discontinuities

within the gradual anisotropic lithology. GPR antennas with frequencies of 10 MHz and 50 MHz were used to ground measurements. In the studied area, the structural data of faults was displayed as pole to fault stereogram and rose diagram. Field geological investigations showed the dominant structural trends as follow: W-E, NE-SW, and NW-SE, which are the result of the local stress on the Dardvey fault in the studied area. Thus the different discontinuity families specified in the C-North deposit were mainly the result of the tectonic and gradual anisotropic lithology. During the GPR survey, the 30 profiles of the C-North deposit were studied in detail. Five GPR and resistivity lines (S12, S24, S25, S26, and S27) were chosen precisely to summarize the most tectonic structures influencing the studied area. The GPR and geological interpretations were simultaneously performed for these profiles. The

fractures and unstable zones identified in the various parts of the C–North deposit must be considered in slope stability studies in order to minimize the risk of instabilities. The detection and monitoring of the mechanical properties such as rock fractures and water content by means of electromagnetic devices can include good results. We integrated the GPR results with the geological data and drill hole log to confirm the sub-surface structures, which later were used for the geological modeling of this area. As a result, a favorable comparison of the GPR results with the geological data lends confidence to the interpretation of the sub-surface structures. To display the entire unstable zones of the studied area, 3D GPR model was built by the processing software package. It was shown that modeling unstable zones as 3D surfaces could be more promising than the typical modeling of fractures as planes. The results obtained showed that the GPR method could improve the way mines manage and minimize the risks associated with slope instability in ore deposits. These results are fundamental for the mining engineers, and provide the basis, and as a guide, for planning the layout of the mine, and to orient the mining front in such a manner as to minimize the operating costs. This work could be considered as the first pilot research work to show the capabilities of GPR for the detection of fractures, unstable zones, and water content zones at an ore deposit in Iran.

### Acknowledgments

This paper is a part of the first author's Ph.D. thesis at Amirkabir University of Technology (AUT), Tehran, Iran. The authors would like to thank the Amirkabir University of Technology (Polytechnic Tehran), Iranian Mines and Mining Industries Development and Renovation Organization (IMIDRO), and Sangan Iron Ore Mines Complex (SIOMC) for supporting this research work (Project NO.95-3-9372). The contributions of Adonis Fard Mousavi, Samira Rezaei, and Nima Jabbari are highly appreciated.

### References

[1]. Acocella, V., Salvini, F., Funicello, R. and Faccenna, C. (1999). The Role of Transfer Structures on Volcanic Activity at Campi Fleigrei (Southern Italy). *Journal of Volcanology and Geothermal Research*. 91: 123-139.

[2]. Noroozi, M., Kakaie, R. and Jalali, S.M.E. (2015). 3D stochastic rock fracture modeling related to strike-slip faults. *Journal of Mining and Environmental*. 7 (2): 169-181.

[3]. Faulkner, D.R., Jackson, C.A.L., Lunn, R.J., Schlische, R.W., Shipton, Z.K., Wibberley, C.A.J. and Withjack, M.O. (2010). A review of recent developments concerning the structure, mechanics and fluid flow properties of fault zones. *Journal of Structural Geology*. 32: 1557-1575.

[4]. Le Garzic, E., L'Hamaide, T., Diraison, M., Géraud, Y., Sausse, J., Urreiztieta, M., Hauville, B. and Champanhet, J. M. (2011). Scaling and geometric properties of extensional fracture systems in the Proterozoic basement of Yemen. Tectonic interpretation and fluid flow implications, *Journal of Structural Geology*. 33: 519-536.

[5]. Elkarmoty, M., Colla, C., Gabrielli, E., Kasmaeeyazdi, S., Tinti, F., Bonduà, S. and Bruno, R. (2017). Mapping and modelling fractures using ground penetrating radar for ornamental stone assessment and recovery optimization: Two case studies. *The Mining-Geology-Petroleum Engineering Bulletin*. 63-76. DOI: 10.17794/rgn.2017.4.7.

[6]. Huaizhi, S., Jinyou, L., Jiping, C. and Zhiping, W. (2014). The macro-comprehensive evaluation method of high rock slope stability in hydropower projects. *Journal of Stochastic Environment Research Risk Assessment*. 28: 213-224.

[7]. Yiping, W., Cong, C., Gaofeng, H. and Zhang, Q. (2014). Landslide stability analysis based on random-fuzzy reliability: taking Liangshuijing landslide as a case. *Journal of Stochastic Environment Research Risk Assessment*. 28: 1723-1732.

[8]. Zanzi, L., Hojat, A., Ranjbar, H., Karimi-Nasab, S., Azadi, A. and Arosio, D. (2017). GPR measurements to detect major discontinuities at Cheshmeh-Shirdoosh limestone quarry, Iran. *Journal of Bulletin Engineering Geology Environment*. DOI: 10.1007/s10064-017-1153-x.

[9]. Arosio, D., Munda, S. and Zanzi, L. (2012). Quality control of stone blocks during quarrying activities. 14<sup>th</sup> International Conference on Ground Penetrating Radar. pp. 822-826.

[10]. Francke, J. (2010). Applications of GPR in mineral resource evaluations. 13<sup>th</sup> International Conference on Ground Penetrating Radar. DOI: 10.1109/ICGPR.2010.5550188

[11]. Luodes, H. (2008). Naturalstoneassessment with ground penetrating radar. *Journal of Earth Science*. 57: 149-155.

[12]. Yelfm, R. J. (2007). Application of Ground Penetrating Radar to Civil and Geotechnical Engineering. *Electromagnetic Phenomena*. V.7, 1 (18): 103-117.

[13]. Gacitua, G., Tamstorf, M., Kristiansen, S. and Uribe, J. (2012). Estimations of moisture content in the active layer in an Arctic ecosystem by using ground-

penetrating radar profiling. *Journal of Applied Geophysics*. 79: 100-106.

[14]. Rashed, M., Kawamura, D., Nemoto, H., Miyata, T. and Nakagawa, K. (2003). Ground penetrating radar investigations across the Uemachi fault, Osaka, Japan. *Journal of Applied Geophysics*. 53: 63-75.

[15]. Pauselli, C., Federico, C., Frigeri, A., Orosei, R., Barchi, M.R. and Basile, G. (2010). Ground penetrating radar investigations to study active faults in the Norcia Basin (central Italy). *Journal of Application Geophysics*. 72: 39-45.

[16]. Yalçiner, C.C., Altunel, E., Bano, M., Meghraoui, M., Karabacak, V. and Serdar, H.I. (2012). Application of GPR to normal faults in the Büyük Menderes Graben, Western Turkey. *Journal of Geodynamics*. 65: 218-227.

[17]. Beauprêtre, S., Garambois, S., Manighetti, I., Malavieille, J., Sénéchal, G., Chatton, M., Davies, T., Larroque, C., Rousset, D., Cotte, N. and Romano, N. (2012). Finding the buried record of past earthquakes with GPR based palaeoseismology: a case study on the Hope fault, New Zealand. *Journal of Geophysics International*. 189: 73-100.

[18]. Ferrero, A.M., Forlani, G., Roncella, R. and Voyat, H.I. (2009). Advanced Geostructural Survey Methods Applied to Rock Mass Characterization. *Rock Mech Rock Eng*. 42: 631-665.

[19]. Francke, J. (2017). Long-range ground penetrating radar for iron ore resource definition. *Iron ore 2017*, Perth, Western Australia.

[20]. Parsanen, A. (2009). The application of ground penetrating radar to the study of Quaternary depositional environments. *Res Terrae, Ser.A No. 29*. Oulu.

[21]. Hänninen, P. (1991). Maatutkaluotaus maaperägeologisissa tutkimuksissa. Summary: Ground penetrating radar in Quaternary geological studies. Report of investigation 103. Geological Survey of Finland. Espoo. 33 P.

[22]. Elkarmoty, M., Colla, C., Gabrieli, E., Papeschi, S. and Bondua, S. (2017). In-situ GPR test for three-dimensional mapping of the dielectric constant in a rock mass. *J. Appl. Geophys*. 146: 1-15.

[23]. Maerz, N.H., Aqeel, A.M. and Anderson, N. (2015). Measuring orientations of individual concealed sub-vertical discontinuities in sandstone rock cuts integrating ground penetrating radar and terrestrial LIDAR. *Environ. Eng. Geosci*. 293-309.

[24]. Elkarmoty, M., Colla, C., Gabrielli, E., Bondua, S. and Bruno, R. (2017). Deterministic three-dimensional rock mass fracture modeling from georadar survey: a case study in a sandstone quarry in Italy. *Environmental and Engineering Geoscience*. 23 (4): 314-331.

[25]. Daniels, D.J. (2004). *Ground Penetrating Radar*, 2<sup>nd</sup> Edition. The Institute of Electrical Engineers, London, United Kingdom.

[26]. Reynolds, J.M. (1997). *An introduction to Applied and Environmental Geophysics*. Wiley, Chichester.

[27]. Reynolds, J.M. (2011). *An introduction to applied and environmental geophysics.*, Second edi, A John Wiley & Sons, Ltd.

[28]. Sepibar, F., Mirnejad, H. and Mi, C. (2018). Mineral chemistry and Ti in zircon thermometry: Insights into magmatic evolution of the Sangan igneous rocks, NE Iran. *Journal of Chemie der Erde*.

[29]. Malekzadeh Shafaroudi, A., Karimpour, M.H. and Golmohammadi, A. (2013). Zircon U-Pb geochronology and petrology of intrusive rocks in the C-North and Baghak districts, Sangan iron mine, NE Iran. *Journal of Asian Earth Sciences*. 64: 256-271.

[30]. Golmohammadi, A., Karimpour, M.H., Malekzadeh Shafaroudi, A. and Mazaheri, S.A. (2015). Alteration-mineralization, and radiometric ages of the source pluton at the Sangan iron skarn deposit, northeastern Iran. *Ore Geol. Rev*. 65 (2): 545-563.

[31]. Kermani, A. and Forster, H. (1991). Petrography, Mineralogical and geochemical investigations of the Sangan Iron ore deposit, northeastern Iran. *Proceedings of Third Mining Symposium of Iran*.

[32]. Mazhari, N., Malekzadeh Shafaroudi, A., Ghaderi, M., Star Lackey, J., Lang Farmer, G. and Karimpour, M.H. (2017). Geochronological and geochemical characteristics of fractionated I-type granites associated with the skarn mineralization in the Sangan mining region, NE Iran.

[33]. Alavi Naini, M. (1982). Geological Quadrangle Map of Khaf: Series Sheet 8059, Ministry of Mines and Metals. Geological survey of Iran, Tehran.

[34]. Mazaheri, A. (1995). Petrological studies of skarns from Marulan south, New south wales, Australia and Sangan, Khorassan, Iran, Univ of Wollongong, Ph.D thesis.

[35]. Shademan, M., Hassani, H., Moarefvand, P. and Madani, H. (2013). Geostatistical assessment of collapses in Gole Gohar open pit mine, Kerman, southwest of Iran, 23rd International Mining Congress & Exhibition of Turkey, ANTALYA, 16-19 April, p.1793-1799.

[36]. Hardcastle, K.C., Emery, J.M., Tinkham, D.J. and Brooks, J.A. (1997). Photolineament Factor Analysis: A new computerized method of remotely assessing the degree to which bedrock is fractured, NWWA Conf. Innov. Ground Water Tech. of the 90's.

[37]. Akinpelu, O.C. (2010). Ground penetrating radar imaging of ancient clastic deposits: A tool for three-dimensional outcrop studies. Ph.D. Thesis, Geology Department, University of Toronto, 374 P.

[38]. Sandmeier, K.J. (2012). The 2D processing and 2D/3D interpretation software for GPR, reflection seismic and refraction seismic. Software catalog 2012, Karlsruhe, Germany.

[39]. DECO Geophysical Co. Ltd. RadExplorer- the software for GPR data processing and interpretation. User manual, Moscow 2005; 92 P.

[40]. Zanzi, L., Hojat, A., Ranjbar, H., Karimi-Nasab, S., Azadi, A. and Arosio, D. (2017). GPR measurements to detect major discontinuities at Cheshmeh-Shiridoosh limestone quarry, Iran. Journal of Bulletin Engineering Geology Environment. DOI: 10.1007/s10064-017-1153-x.

[41]. Luodes, H., Sutinen, H. and Härmä, P. (2006). Characterization of fracturing in rapakivi granite with GPR. In: Cardu, M., Ciccu, R., Lovera, E. & Michelotti, E. (eds). Proceedings of The Fifteenth International Symposium on Mine Planning and Equipment Selection. Torino. Italy. 20-22 September 2006.

[42]. Luodes, H. and Sutinen, H. (2011). Evaluation and modelling natural stone rock quality using ground penetrating radar. In: Nenonen, K. & Nurmi, P. A. (eds) Geoscience for society. 125th anniversary volume. Geological Survey of Finland. Special Paper. 49: 83-90.

## تعیین مناطق ناپایدار تکتونیکی در ذخیره C شمالی، سنگان، شمال شرق ایران با استفاده از روش رادار نفوذی زمین (GPR): اهمیت زمین‌شناسی ساختاری

علی رضایی<sup>۱</sup>، حسین حسینی<sup>۱\*</sup>، پرویز معارف‌وند<sup>۱</sup> و عباس گل‌محمدی<sup>۲</sup>

۱- دانشکده مهندسی معدن و متالورژی، دانشگاه صنعتی امیرکبیر (پلی تکنیک تهران)، ایران

۲- سازمان زمین‌شناسی و اکتشافات معدنی کشور، تهران، ایران

ارسال ۲۰۱۸/۸/۱۹، پذیرش ۲۰۱۹/۱/۱۴

\* نویسنده مسئول مکاتبات: [hhassani@aut.ac.ir](mailto:hhassani@aut.ac.ir)

### چکیده:

رادار نفوذی زمین (GPR)، یک روش ژئوفیزیکی مؤثر و کاربردی با یک طیف وسیعی از کاربردها در نقشه‌برداری زمین‌شناسی برای به دست آوردن اطلاعات زیرسطحی است. هدف از این پژوهش، تعیین تفاوت‌های پارامتر ژئوفیزیکی در ساختارهای زمین‌شناسی زیرسطحی و ساخت مدل شکستگی سه بعدی است. روش‌های رادار نفوذی زمین و مقاومت‌سنجی برای شناسایی مناطق ناپایدار تکتونیکی در ذخیره C شمالی به کار برده شده است. ابتدا بررسی‌های زمین‌شناسی ساختاری برای شناسایی گسل‌ها و شکستگی‌ها در منطقه مورد مطالعه انجام شده است. بر اساس ویژگی‌های ساختاری به دست آمده، این بررسی بر روی یک ناحیه به مساحت یک کیلومتر مربع با مجموع ۳۰ پروفیل برای شناسایی مناطق کم مقاومت در ذخیره C شمالی انجام شده است که کمک شایانی در کاهش مشکلات مربوط به مطالعه پایداری شیب خواهد کرد. سپس پروفیل‌های رادار نفوذی زمین با آنتن‌های فرکانس پایین و بالا (۱۰ و ۵۰ مگاهرتز) برای شناسایی شکستگی‌ها و مناطق آبدار طراحی شده‌اند. نتایج به دست آمده نشان می‌دهد که روند عمده ساختاری در منطقه مورد مطالعه، شرقی- غربی، شمال شرق- جنوب غرب و شمال غرب- جنوب شرق است، در حالی که مناطق گسلی می‌توانند مسیرهایی برای ورود آب‌های زیرزمینی به داخل ذخیره معدنی در آینده ایجاد کنند. همچنین اطلاعات به دست آمده از مطالعات زمین‌شناسی و رادار نفوذی زمین، با اطلاعات گمانه‌های حفاری تلفیق و اعتبارسنجی شده‌اند. اطلاعات زمین‌شناسی ساختارها با وضعیت واقعی زمین‌شناسی در زیر سطح در تطابق کامل است. روش و نتایج این کار می‌تواند در حل مسائل مربوط به ساختارهای زیرسطحی در مهندسی معدن مفید باشد.

**کلمات کلیدی:** ساختارهای زمین‌شناسی، رادار نفوذی زمین، مقاومت‌سنجی، مدل‌سازی، ذخیره C شمالی، سنگان، ایران.